A Raman spectroscopic study of thermally treated glushinskite –the natural magnesium oxalate dihydrate

Ray L. Frost•, Moses Adebajo, Matt L. Weier

Inorganic Materials Research Program, Queensland University of Technology, 2 George Street, Brisbane, GPO Box 2434, Queensland 4001, Australia.

Published as:
Frost, R., Adebajo, M. & Weier M, A Raman spectroscopic study of thermally treated glushinskite--the natural magnesium oxalate dihydrate. Spectrochimica acta. Part A, Molecular and biomolecular spectroscopy, 2004. 60(3): p. 643-51.

Abstract

Raman spectroscopy has been used to study the thermal transformations of natural magnesium oxalate dihydrate known in mineralogy as glushinskite. The data obtained by Raman spectroscopy was supplemented with that of infrared emission spectroscopy. The vibrational spectroscopic data was complimented with high resolution thermogravimetric analysis combined with evolved gas mass spectrometry. TG-MS identified three mass loss steps at 146 and 397 °C. In the first mass loss step water is evolved only, in the second step carbon dioxide is evolved. The combination of Raman microscopy and a thermal stage clearly identifies the changes in the molecular structure with thermal treatment. Glushinskite is the di-hydrate phase in the temperature range up to the pre-dehydration temperature of 146 °C. Above 397 °C, magnesium oxide is formed. Infrared emission spectroscopy shows that this mineral decomposes at around 400 °C. Changes in the position and intensity of the CO and CC stretching vibrations in the Raman spectra indicate the temperature range at which these phase changes occur.

*Keywords***:** oxalate, glushinskite, infrared emission, Raman spectroscopy, thermogravimetry

---

1. Introduction

Glushinskite is a naturally occurring magnesium oxalate dihydrate [1-3]. The mineral is of importance as it can be formed by lichens, fungi and other plants by the uptake and subsequent expulsion of the magnesium cation [4]. Glushinskite may be termed a biomineral since it is found as a waste product in litter decomposition [5, 6]. The presence of glushinskite and the other calcium oxalates known as weddellite and whewellite are indicators of biodegeneration in land fills and sediments [7]. The presence of glushinskite can be used as indicators of climatic change in times past [8]. Studies of monument degradation show the presence of oxalates as one of the prime biominerals in their deterioration [9-12]. The presence of the oxalate will depend on the chemical composition of the mineral used in the construction of the edifice which

• Author to whom correspondence should be addressed (r.frost@qut.edu.au)

more than not will be a marble or limestone. Magnesium content in these materials will result in glushinskite formation. Glushinskite is one of many possible minerals that may be formed in kidney and urinary tracts [13-23].

Thermal studies have been known for some considerable time [24-26]. Differential mass changes were followed as a function of time for synthetic magnesium dihydrate [25]. Mechanisms for the solid-state decomposition reactions of magnesium oxalate dihydrate as well as corresponding activation energy values calculated according to a thermogravimetric method were reported [27]. Infrared emission spectroscopy has been used to follow the thermal decomposition of magnesium oxalate dihydrate [28, 29]. The kinetics of decomposition of the synthetic glushinskite has been studied [30]. It was found that the dehydration of $MgC_2O_4.2H_2O$ was governed by Avrami-Erofeev nuclei growth [30]. The activation energy and the pre-exponential factor vary with temperature over wide temperature ranges. Both anhydrous oxalates dissociated to the carbonates according to the Avrami-Erofeev nuclei growth, A2. For magnesium oxalate, at low heating rates, this step was accompanied by dissociation. of $MgCO_3$ to MgO. The kinetics of isothermal dehydration of $MgC_2O_4.2H_2O$ in a dry nitrogen was studied by TG [31]. One method of producing mixed oxide catalysts is to thermally treat the metal oxalates [32]. In this way mixed metal oxides mixed at the atomic level are produced. There have been no recent studies of the thermal decomposition of glushinskite and certainly no Raman spectroscopic studies of thermal treated glushinskite.

2. Experimental

2.1 Mineral:

The glushinskite was obtained from the South Australian museum. The samples were phase analyzed using X-ray diffraction and the compositions checked using EDX measurements.

2.2 Thermal Analysis

Thermal decomposition of the natural oxalate was carried out in a TA® Instruments incorporated high-resolution thermogravimetric analyzer (series Q500) in a flowing nitrogen atmosphere (80 cm^3/min). Approximately 50mg of sample was heated in an open platinum crucible at a rate of 5.0 °C/min up to 500°C. With the quasi-isothermal, quasi-isobaric heating program of the instrument the furnace temperature was regulated precisely to provide a uniform rate of decomposition in the main decomposition stage. The TGA instrument was coupled to a Balzers (Pfeiffer) mass spectrometer for gas analysis. Only selected gases were analyzed.

2.3 Raman microprobe spectroscopy

The crystals glushinskite were placed and orientated on the stage of an Olympus BHSM microscope, equipped with 10x and 50x objectives and part of a Renishaw 1000 Raman microscope system, which also includes a monochromator, a filter system and a Charge Coupled Device (CCD). Raman spectra were excited by a HeNe laser (633 nm) at a resolution of 2 cm^{-1} in the range between 100 and 4000

cm^{-1}. Repeated acquisition using the highest magnification was accumulated to improve the signal to noise ratio. Spectra were calibrated using the 520.5 cm^{-1} line of a silicon wafer. In order to ensure that the correct spectra are obtained, the incident excitation radiation was scrambled. Previous studies by the authors provide more details of the experimental technique. Spectra at liquid nitrogen temperature were obtained using a Linkam thermal stage (Scientific Instruments Ltd, Waterfield, Surrey, England).

2.4 Infrared emission spectroscopy

Details of infrared emission spectroscopy has been previously published [33, 34]. Spectroscopic manipulation such as baseline adjustment, smoothing and normalisation were performed using the Spectracalc software package GRAMS (Galactic Industries Corporation, NH, USA). Band component analysis was undertaken using the Jandel 'Peakfit' software package, which enabled the type of fitting, function to be selected and allows specific parameters to be fixed or varied accordingly. Band fitting was done using a Gauss-Lorentz cross-product function with the minimum number of component bands used for the fitting process. The Gauss-Lorentz ratio was maintained at values greater than 0.7 and fitting was undertaken until reproducible results were obtained with squared correlations of r^2 greater than 0.995.

3. Results and discussion

The HRTG and mass spectrometric curves for glushinskite are shown in Figure 1. The thermal decomposition of glushinskite shows two steps with mass losses at 148 and 397 °C of 22.8% and 46.6%. These values correspond with a theoretical mass loss of 24.3 and 48.5% which is in good agreement with the experimental values. It is proposed that the weight loss steps occur according to the following reactions:

Step 1
$MgC_2O_4.2H_2O \rightarrow MgC_2O_4 + 2H_2O$
Step 2
$MgC_2O_4 \rightarrow MgO + CO + CO_2$

The thermal decomposition of glushinskite occurs via two steps by conversion of the magnesium oxalate hydrate to the anhydrous compound and then the decomposition of the oxalate to the magnesium oxide and carbon monoxide and carbon dioxide. Although there is no evidence for the breakdown of the last step into two successive steps, it is possible that the magnesium oxalate decomposed to magnesium carbonate and carbon monoxide with the successive breakdown of the magnesium carbonate to magnesium oxide and carbon dioxide. The use of vibrational spectroscopy may assist in the analysis of this reaction. The values for the mass loss steps are in agreement with the previously published data [35, 36]. The thermal analysis of magnesium oxalate is often obtained by its measurement in mixtures with calcium or manganese oxalates [30]. Mass spectrometry of the evolved gases through the thermal treatment of glushinskite (shown in Figure 1b) confirms that water vapour is evolved over the 136 to 175 °C temperature range and peaks at 146 °C and that both water and carbon dioxide are evolved simultaneously over the temperature range 222 to 360 °C. A

second carbon dioxide evolution takes place over the 362 to 444 °C temperature range.

The Raman spectra of the hydroxyl stretching region of thermally treated glushinskite are shown in Figure 2. The results of the Raman spectral analysis are reported in Table 1. A single band is observed at 3370 cm^{-1} at 50 °C, 3372 cm^{-1} at 100 °C, 3375 cm^{-1} at 150 °C and 3379 cm^{-1} at 200 °C. The peak positions of hydroxyl stretching show a red shift with thermal treatment. No intensity is observed in the bands above 200 °C. The results of the Raman spectra of the hydroxyl stretching region of glushinskite are in agreement with the results of the TG and MS of glushinskite. These results are supplemented by the infrared emission spectra (Figure 3). The most intense emission band is observed at 3388 cm^{-1} with other low intensity bands observed at 3230, 3164 and 2985 cm^{-1}. This latter band may simply indicate the presence of some organic impurities in the mineral. Some intensity remains in the 3388 cm^{-1} band at 150 °C and approaches zero at 175 °C. This result is in line with the Raman data. The band in the Raman and the band in the infrared spectrum are not the same band. The band at 3370 cm^{-1} in the Raman spectrum is attributed to the OH symmetric stretching mode whereas the band at 3380 in the IE spectra is assigned to the OH antisymmetric stretching mode.

The Raman spectra in the 1300 to 1800 cm^{-1} region for the thermal treatment of glushinskite is shown in Figure 4. This region is the region of observation of the CO stretching vibration. A band is identified at 1449 cm^{-1} for potassium oxalate in the solid state. The Raman spectrum of the mineral glushinskite shows a band at 1471 cm^{-1} in the 298 K spectrum. Mild heating results in the observation of two bands at 1448 and 1470 cm^{-1}; the latter being a very intense band. These bands remain in these positions up to 175 °C. Above this temperature the bands shift to 1454 and 1497 cm^{-1}. These bands are assigned to the $\nu_{(C\text{-}O)}$ stretching mode. The intensity of these bands decrease up to 600 °C, after which temperature no intensity remains in any of the bands. For aqueous oxalate the antisymmetric stretching (B_{2u}) mode is observed at 1600 cm^{-1}. Low intensity bands are observed at 1637, 1659 and 1724 cm^{-1} and are assigned to this mode. These bands decrease in intensity up to 200 °C, after which only a single band at 1683 cm^{-1} is observed.

Published IR data suggests that there should be a single band at 1632 cm^{-1} [37]. Figure 5 shows the infrared emission spectra over the 1000 to 2000 cm^{-1} range. For glushinskite infrared bands are observed at 298 K at 1679, 1660, 1634 and 1603 cm^{-1}. At 75 °C, three bands are distinguished at 1662, 1641 and 1614 cm^{-1}. The bands are present in the 100 and 125 °C spectra but above this temperature a broad profile is observed centred upon 1664 cm^{-1}. An additional band which is not in the room temperature, 75 and 100 °C spectra is observed at 1486 cm^{-1}. This band, although decreasing in intensity is present up to 400 °C. The presence of this band is of significance, in that it is the normally forbidden symmetric stretching mode. For centrosymmetric molecules there is the rule of mutual exclusion in that bands observed in the infrared and not observed in the Raman spectra and the reverse. This means that thermal treatment has caused the non-planarity of the oxalate. The infrared spectra show quite intense bands centred around 1300 cm^{-1}. These bands may be assigned to B_{3u} OCO stretching modes. Two bands are observed at 1373 and 1324 cm^{-1}. The intensity of these bands decreases with thermal treatment.

The Raman spectra of the C-C stretching region of glushinskite up to 600 °C are shown in Figure 6. After this temperature no intensity is observed in the band indication the glushinskite has been thermally decomposed. The position of the band is observed at around 888 cm^{-1} for potassium oxalate. It is noted that there is a large shift in this band for glushinskite. The band shows a small red shift with thermal treatment. The band is observed at 922 cm^{-1} in the 550 °C spectrum. The Raman spectra of the oxalate minerals all show a low intensity band at around 860 cm^{-1}. The band is assigned to the OCO bending mode. A band is not observed in this position for potassium oxalate. The band is observed at 861 °C at 50 °C and shows a decrease in band position with temperature increase. The band is observed at 849 cm^{-1} at 250 °C and at 851 cm^{-1} at 550 °C. There appears to be an abrupt change in position after 250 °C. No bands are observed in these positions in the infrared emission spectra. Infrared emission bands are observed at 828 and 804 cm^{-1}. Both bands show a blue shift with increasing temperature (Figure 7). The bands are still present at 450 °C. The band shows no intensity at 475 °C. No band is observed in the Raman spectra at this position. The band is attributed to an out-of-plane bending mode. The equivalent band may well be the low intensity band observed in the Raman spectra at 861 °C.

The Raman spectra of the low wavenumber region of glushinskite are shown in Figure 8. Two bands are observed at 585 and 527 cm^{-1}. The intensity of the band at 585 cm^{-1} approaches zero by 200 °C. The band is assigned to the water librational mode. The band at 527 cm^{-1} is assigned to a MO stretching and MO ring modes. Previous studies have assigned the band at around 500 cm^{-1} to the bending mode of C-C-O and the MO ring and MO stretching modes [38, 39]. The band at around 596 cm^{-1} is also associated with MO stretching modes [38, 39]. The Raman spectra of the very low wavenumber region are shown in Figure 9. A number of intense bands are observed between 200 and 300 cm^{-1} for these natural oxalates. Raman spectroscopy does have the advantage that bands below 400 cm^{-1} are readily obtained. This is important to the study of oxalates as the MgO stretching and OMO ring bending modes may be determined. In the Raman spectrum of glushinskite bands are observed at 309, 265 and 227 cm^{-1}. These bands are probably attributable to MgO ring stretching or bending modes. The band at 309 shifts to 305 cm^{-1} and the intensity is lost by 150 °C. This band is considered be associated with water vibrations. The band at 265 cm^{-1} changes abruptly to 242 cm^{-1} at 200 °C. This band shows a slight red shift with thermal treatment.

4. Conclusions

A combination of Raman and infrared emission spectroscopy has been used to study the thermal decomposition of a natural sample of glushinskite. The Raman spectra were obtained using a combination of Raman microscopy in combination with a thermal stage. Infrared emission spectra were obtained by collecting spectra in situ at the elevated temperatures by using the hot sample as the emission source. The spectroscopic data was complimented by high resolution thermogravimetric analysis in combination with evolved gas mass spectrometry. Both sets of spectral data show changes in the molecular structure as a function of temperature. The Raman and infrared spectra are mutually exclusive showing that structure of glushinskite is bidentate and planar at temperatures below 200 °C. However the mutual exclusivity

is lost above this temperature, suggesting the planarity of the molecule is lost with thermal treatment.

Thermal analysis shows that a weight loss step occurs over the 140 to 154 °C temperature range and mass spectrometry proves that this weight loss step is associated with water loss. Complexity exists in the vibrational spectra of glushinskite with thermal treatment. The observation of a complex set of overlapping bands shows that more than one type of water is present and that dehydration may take place at low temperatures. The phase change at 148 °C results in the formation of anhydrous magnesium oxalate which above 397 °C converts to magnesium oxide. These phase changes can be readily followed by Raman spectroscopy and infrared emission spectroscopy. Shifts in the band positions of the symmetric stretching modes provide details of the changes in molecular structure during these phase changes.

Acknowledgments

The financial and infra-structure support of the Queensland University of Technology Inorganic Materials Research Program is gratefully acknowledged. The Australian Research Council (ARC) is thanked for funding. Prof Allan Pring of the South Australian Museum is thanked for the loan of the oxalate mineral.

References

[1]. M. J. Wilson and P. Bayliss, Mineralogical Magazine 51 (1987) 327.
[2]. M. J. Wilson, D. Jones and J. D. Russell, Mineralogical Magazine 43 (1980) 837.
[3]. U. M. Cowgill, Mineralogical Magazine 53 (1989) 505.
[4]. R. E. Crick, B. Burkart, J. A. Chamberlain, Jr. and K. O. Mann, Journal of the Marine Biological Association of the United Kingdom 65 (1985) 415.
[5]. H. J. Arnott, Scanning Electron Microsc. (1982) 1141.
[6]. U. M. Cowgill and G. T. Prance, Annals of Botany (Oxford, United Kingdom) 64 (1989) 697.
[7]. D. A. C. Manning, Journal of the Geological Society (London) 157 (2000) 229.
[8]. S. Moore, M. J. Beazley, M. R. Mccallum and J. Russ, Preprints of Extended Abstracts presented at the ACS National Meeting, American Chemical Society, Division of Environmental Chemistry 40 (2000) 4.
[9]. M. Del Monte and C. Sabbioni, Environ. Sci. Technol. 17 (1983) 518.
[10]. M. Del Monte and C. Sabbioni, Science of the Total Environment 50 (1986) 165.
[11]. M. Del Monte, C. Sabbioni and G. Zappia, Science of the Total Environment 67 (1987) 17.
[12]. A. Piterans, D. Indriksone, A. Spricis and A. Actins, Proceedings of the Latvian Academy of Sciences, Section B: Natural, Exact and Applied Sciences 51 (1997) 254.
[13]. M. Afzal, M. Iqbal and H. Ahmad, Journal of Thermal Analysis 38 (1992) 1671.
[14]. R. Asper and O. Schmucki, Urologia Internationalis 41 (1986) 334.

[15]. W. Berg, P. Brundig, C. Bothor and H. J. Schneider, Int. Urol. Nephrol. 14 (1982) 363.
[16]. G. J. Beukes, H. De Bruiyn and W. J. H. Vermaak, British Journal of Urology 60 (1987) 387.
[17]. M. Diaz-Espineira, E. Escolar, J. Bellanato and J. A. Medina, Scanning Microscopy 9 (1995) 1071.
[18]. A. Hesse, G. Sanders and D. B. Leusmann, Scanning Electron Microscopy (1986) 1705.
[19]. T. S. Mair and R. S. Osborn, Research in Veterinary Science 40 (1986) 288.
[20]. C. Paluszkiewicz, M. Galka, W. Kwiatek, A. Parczewski and S. Walas, Biospectroscopy 3 (1997) 403.
[21]. G. Schubert and G. Brien, Int. Urol. Nephrol. 13 (1981) 249.
[22]. K. Sudlow and A. Woolf, Clinica Chimica Acta 203 (1991) 387.
[23]. K. Tozuka, T. Konjiki and T. Sudo, J. Urol. (Baltimore) 130 (1983) 1119.
[24]. H. Schmittler, Monatsberichte der Deutschen Akademie der Wissenschaften zu Berlin 9 (1967) 445.
[25]. A. V. Shkarin, N. D. Topor and G. M. Zhabrova, Kinetika i Kataliz 8 (1967) 1377.
[26]. A. V. Shkarin, G. M. Zhabrova, N. D. Topor and M. Y. Kushnarev, Izvestiya Tomskogo Politekhnicheskogo Instituta 199 (1969) 105.
[27]. M. I. Zaki and M. Abdel-Khalik, Thermochimica Acta 78 (1984) 29.
[28]. G. Fabbri and P. Baraldi, Atti della Societa dei Naturalisti e Matematici di Modena 106 (1975) 81.
[29]. G. Fabbri and P. Baraldi, Atti della Societa dei Naturalisti e Matematici di Modena 106 (1975) 57.
[30]. A. M. M. Gadalla, Thermochimica Acta 74 (1984) 255.
[31]. Y. Masuda, K. Iwata, R. Ito and Y. Ito, Journal of Physical Chemistry 91 (1987) 6543.
[32]. J. A. Wang, A. Morales, X. Bokhimi, O. Novaro, T. Lopez and R. Gomez, Chemistry of Materials 11 (1999) 308.
[33]. R. L. Frost, Z. Ding, J. T. Kloprogge and W. N. Martens, Thermochimica Acta 390 (2002) 133.
[34]. R. L. Frost, Z. Ding, W. N. Martens and T. E. Johnson, Thermochimica Acta 398 (2003) 167.
[35]. E. Wiederholt, V. Fahrney and R. Skrozki, Journal of Thermal Analysis 35 (1989) 541.
[36]. J. Mu and D. D. Perlmutter, Thermochimica Acta 49 (1981) 207.
[37]. H. G. M. Edwards, D. W. Farwell, R. Jenkins and M. R. D. Seaward, Journal of Raman Spectroscopy 23 (1992) 185.
[38]. H. G. M. Edwards, D. W. Farwell, S. J. Rose and D. N. Smith, Journal of Molecular Structure 249 (1991) 233.
[39]. R. I. Bickley, H. G. M. Edwards and S. J. Rose, Journal of Molecular Structure 243 (1991) 341.

	50	100	150	200	250	300	350	400	450	
centre	3476	3476								
area	0.003	0.002								
centre	3368	3370	3372	3373	3401					
area	0.160	0.135	0.119	0.095	0.023					
centre	3265		3258	3266						
area	0.011		0.008	0.011						
centre	3191									
area	0.005									
centre	2903	2903	2903	2903	2902	2903		2903	2903	
area	0.011	0.006	0.007	0.005	0.008	0.009		0.006	0.012	
centre						2680				
area						0.004				
centre								1778		
area								0.054		
centre	1720	1720	1719	1719						
area	0.003	0.004	0.003	0.005						
centre	1659	1659	1658	1657	1680	1678	1678	1679	1676	1
area	0.013	0.012	0.012	0.013	0.078	0.053	0.076	0.030	0.109	0
centre	1636	1636	1635	1634	1640					
area	0.043	0.051	0.044	0.040	0.013					
centre					1499	1499	1498	1495	1495	1
area					0.092	0.115	0.112	0.196	0.222	0
centre					1491	1488	1488	1477	1475	1
area					0.236	0.093	0.065	0.153	0.181	0
centre	1471	1471	1470	1470	1459	1475	1475			
area	0.157	0.135	0.115	0.122	0.099	0.219	0.185			
centre	1465	1466	1466	1465						
area	0.126	0.142	0.142	0.155						
centre	1443	1441	1440	1438						
area	0.060	0.068	0.065	0.062						
centre						1150	1188	1300		
area						0.034	0.010	0.023		
centre										
area										
centre					926	927	925		927	
area					0.067	0.057	0.078		0.018	
centre	916	915	914	913	913	916	914	922	921	
area	0.093	0.090	0.078	0.099	0.048	0.055	0.040	0.158	0.122	0
centre	883									
area	0.009									
centre	861	861	862	862	849	851	851	850	852	
area	0.002	0.004	0.004	0.004	0.032	0.019	0.022	0.036	0.013	0
centre						833	832			
area						0.007	0.008			
centre										
area										
centre								695		
area								0.069		
centre				651	624	619	630			
area				0.011	0.035	0.053	0.011			
centre	585	584	583	582						

area	0.034	0.034	0.036	0.046						
centre	527	526	525	525	537	530	529	527	528	
area	0.140	0.130	0.125	0.083	0.080	0.123	0.107	0.121	0.182	0
centre		511	511	520	526					
area		0.025	0.030	0.051	0.065					0
centre										
area										
centre								388		
area								0.034		
centre		309	305							
area		0.015	0.005							
centre										
area										
centre	265	264	263	262						
area	0.037	0.015	0.034	0.015						
centre					242	242	242	239	241	
area					0.046	0.052	0.051	0.049	0.044	0
centre	227	227	227	226	221	221	223			
area	0.054	0.062	0.092	0.082	0.021	0.037	0.064			
centre								206	208	
area								0.004	0.044	0

Table 1 Results of the Raman spectral analysis of thermally treated glushinskite

75°C	100°C	125°C	150°C	175°C	200°C	250°C	300°C	350°C	375°C
	1949	**1921**	**1932**	**1934**	**1932**	**1937**	**1923**	**1911**	**1943**
	0.002	0.006	0.011	0.006	0.008	0.004	0.011	0.012	0.001
1909	**1907**								**1851**
0.014	0.013								0.002
1690	**1691**	**1714**	**1730**	**1731**	**1731**	**1731**	**1728**	**1722**	**1719**
0.144	0.187	0.139	0.061	0.057	0.064	0.066	0.079	0.102	0.114
1659	**1658**	**1662**	**1673**	**1673**	**1674**	**1668**	**1663**	**1661**	**1659**
0.162	0.163	0.270	0.383	0.415	0.394	0.418	0.443	0.415	0.408
1636	**1636**	**1634**	**1623**	**1623**	**1624**	**1623**	**1609**	**1598**	**1594**
0.035	0.023	0.003	0.173	0.135	0.155	0.102	0.043	0.030	0.027
1610	**1611**	**1615**							
0.265	0.227	0.191							
1370		**1473**	**1475**	**1475**	**1475**	**1476**	**1477**	**1478**	**1478**
0.059		0.023	0.036	0.037	0.034	0.018	0.008	0.003	0.003
1322	**1370**	**1373**	**1376**	**1378**	**1377**	**1378**	**1377**	**1377**	**1377**
0.168	0.058	0.048	0.049	0.052	0.058	0.069	0.079	0.085	0.090
1184	**1321**	**1322**	**1322**	**1322**	**1322**	**1320**	**1319**	**1318**	**1317**
0.017	0.172	0.184	0.184	0.194	0.181	0.219	0.223	0.235	0.226
1134	**1182**	**1181**	**1184**	**1183**	**1182**	**1181**	**1171**	**1161**	**1163**
0.021	0.023	0.016	0.005	0.005	0.005	0.004	0.008	0.010	0.012
974	**1132**	**1132**	**1129**	**1130**	**1128**	**1127**	**1133**	**1129**	**1129**
0.009	0.014	0.010	0.003	0.004	0.005	0.005	0.003	0.006	0.007
938	**973**	**969**	**974**	**974**	**974**	**975**	**975**	**980**	**979**
0.009	0.012	0.008	0.002	0.001	0.002	0.002	0.002	0.002	0.003
827	**933**	**928**	**923**	**921**	**919**	**921**	**921**	**920**	**922**
0.039	0.013	0.015	0.009	0.008	0.007	0.007	0.006	0.004	0.006
			859	**858**	**858**	**857**			
			0.002	0.003	0.002	0.000			
	828	**828**	**825**	**822**	**824**	**814**	**816**	**809**	
	0.064	0.022	0.028	0.020	0.020	0.029	0.011	0.011	
	804	**803**	**802**	**801**	**802**	**801**	**801**	**799**	**801**
	0.012	0.034	0.028	0.033	0.034	0.030	0.038	0.079	0.103
691	**689**	**689**	**687**	**684**	**684**	**684**			
.012	0.009	0.004	0.001	0.000	0.000	0.000			

Table 2 Results of the infrared emission spectra of glushinskite

List of Figures

List of Tables

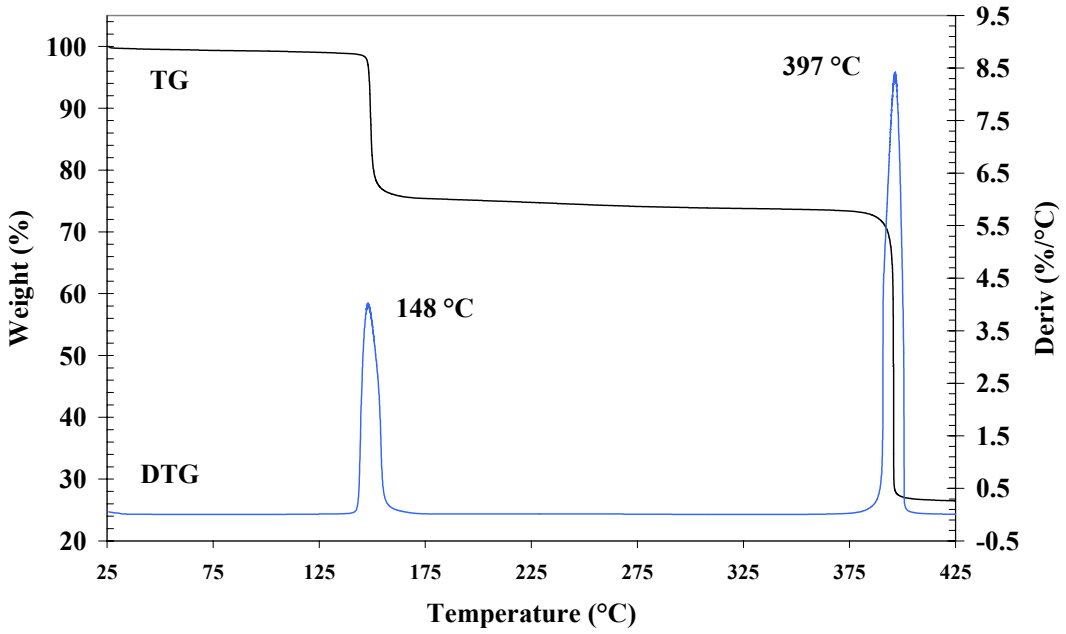

Figure 1a

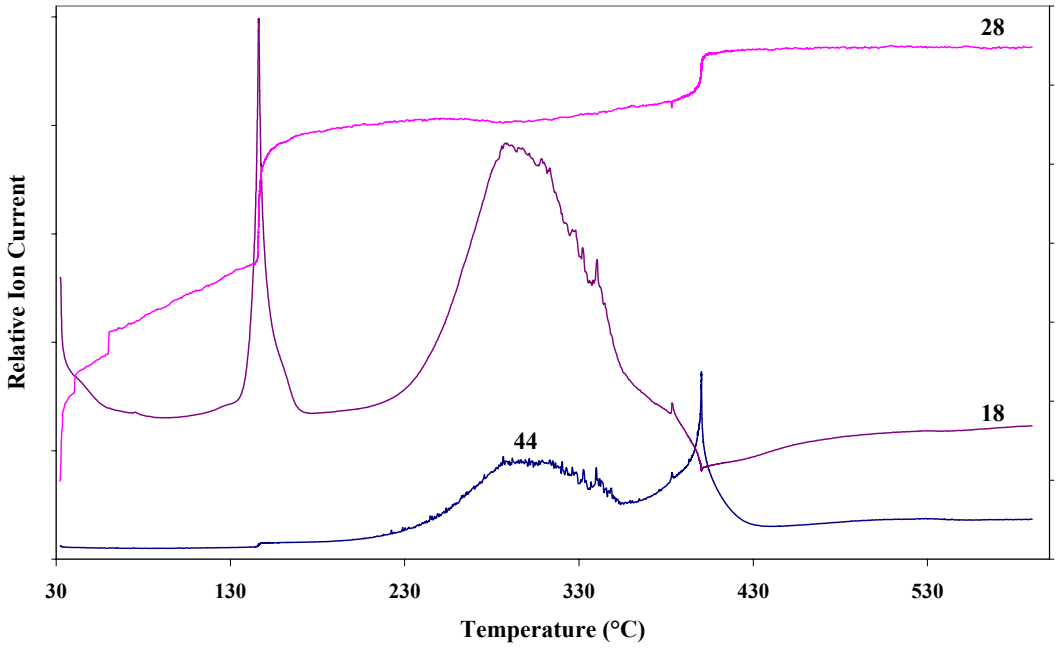

Figure 1b

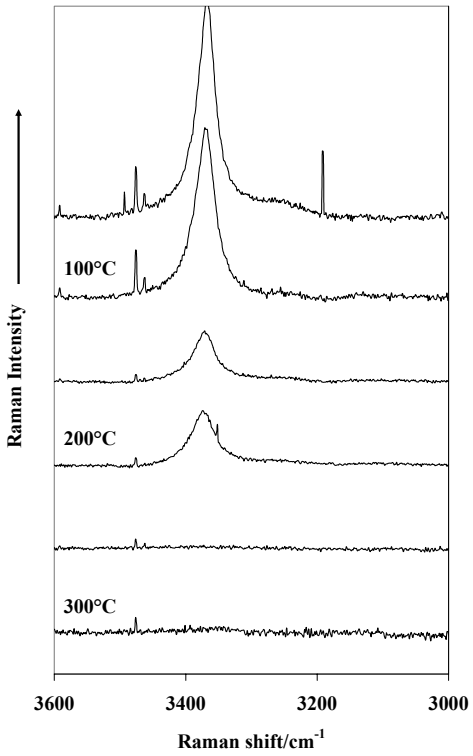
Raman Intensity
100°C
200°C
300°C
3600
3400
3200
3000
Raman shift/cm-1

Figure 2

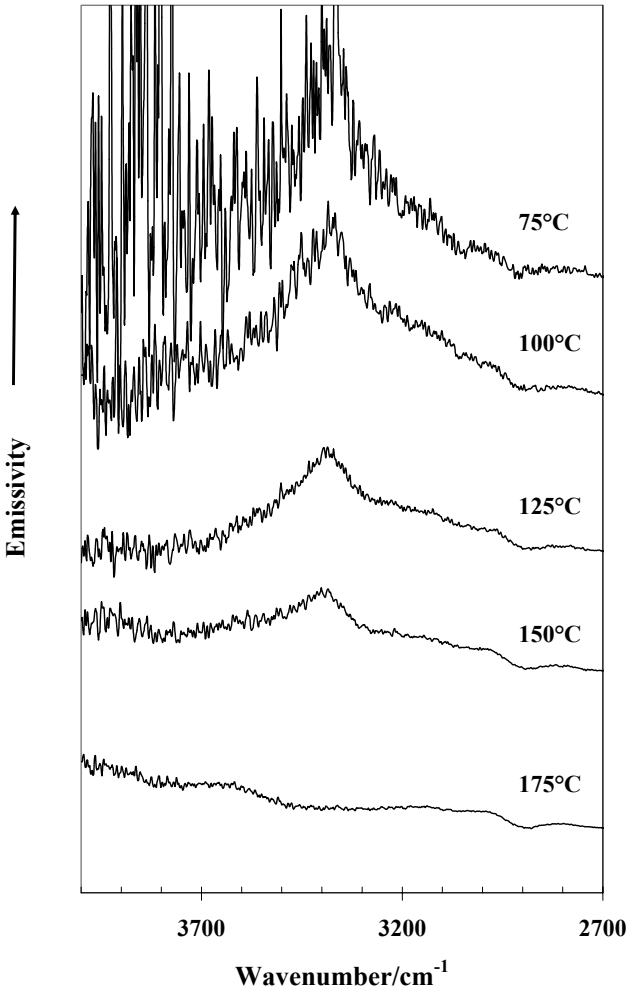
75°C
100°C
125°C
150°C
175°C
Emissivity
3700
3200
2700
Wavenumber/cm-1

Figure 3

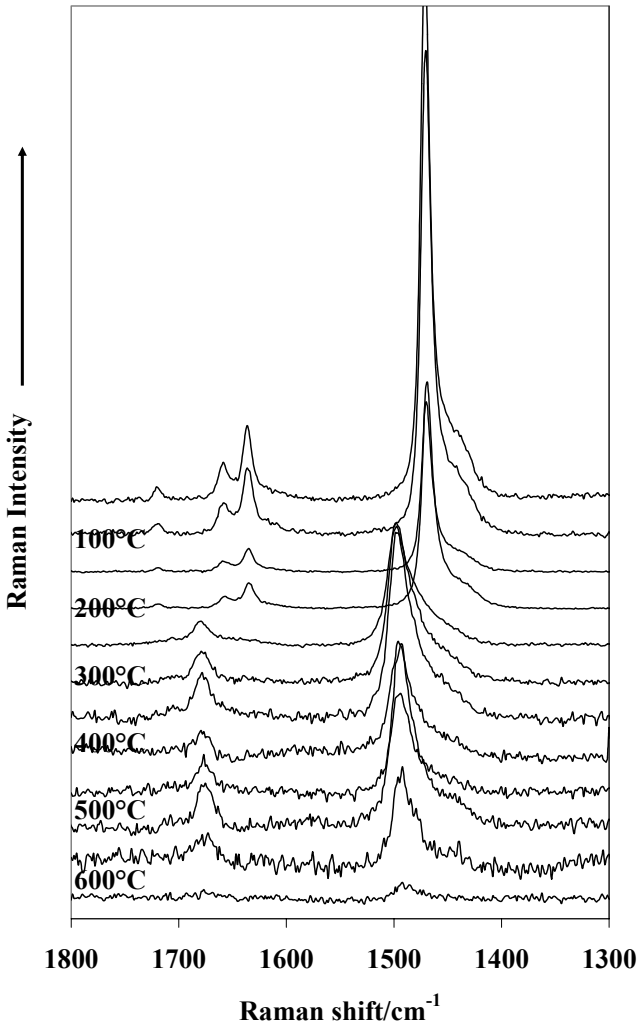
Raman Intensity
100°C
200°C
300°C
400°C
500°C
600°C
1800
1700
1600
1500
1400
1300
Raman shift/cm-1

Figure 4

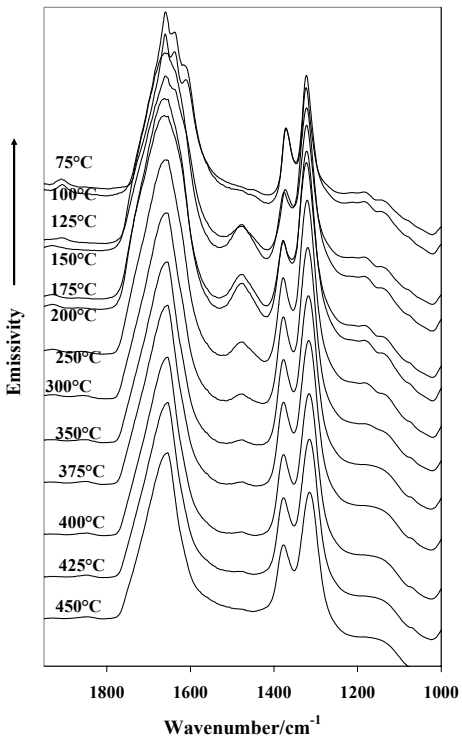
75°C
100°C
125°C
150°C
175°C
200°C
250°C
300°C
350°C
375°C
400°C
425°C
450°C
Emissivity
1800
1600
1400
1200
1000
Wavenumber/cm-1

Figure 5

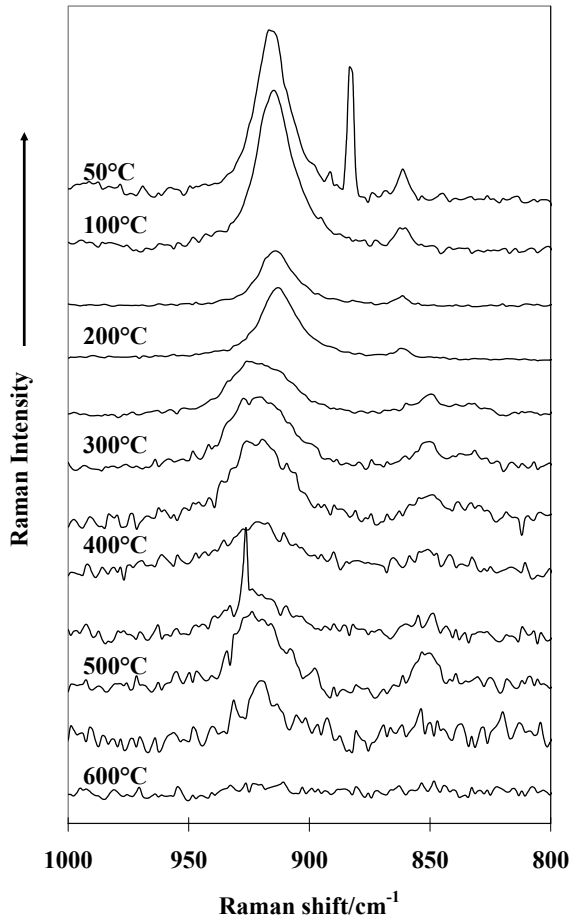
50°C
100°C
200°C
300°C
400°C
500°C
600°C
Raman Intensity
1000
950
900
850
800
Raman shift/cm-1

Figure 6

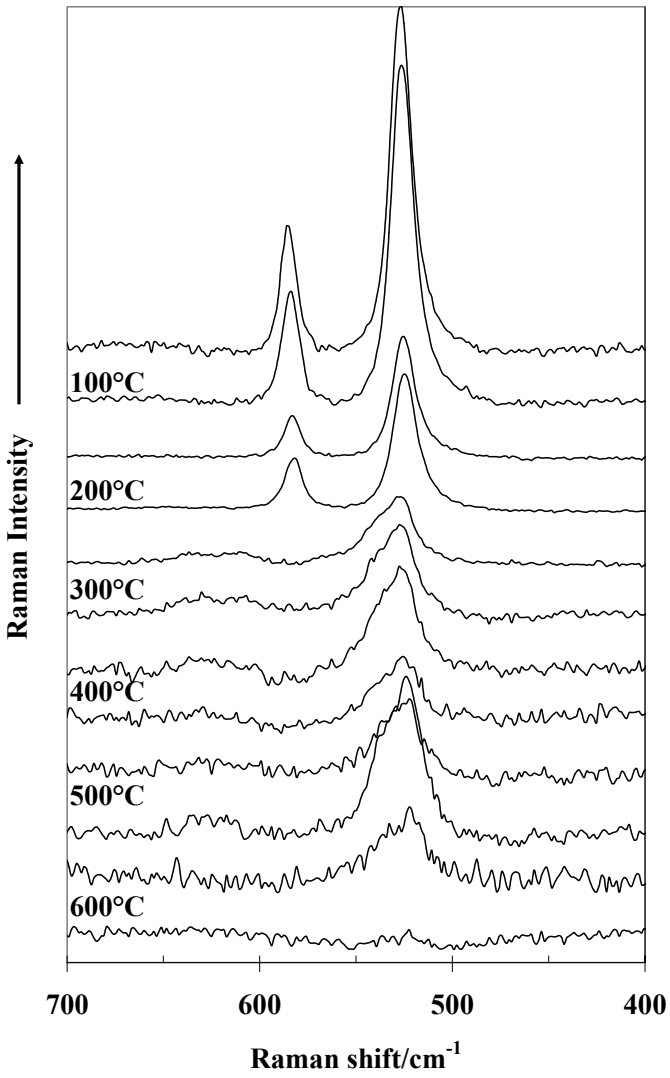
Raman Intensity
100°C
200°C
300°C
400°C
500°C
600°C
700
600
500
400
Raman shift/cm-1

Figure 8

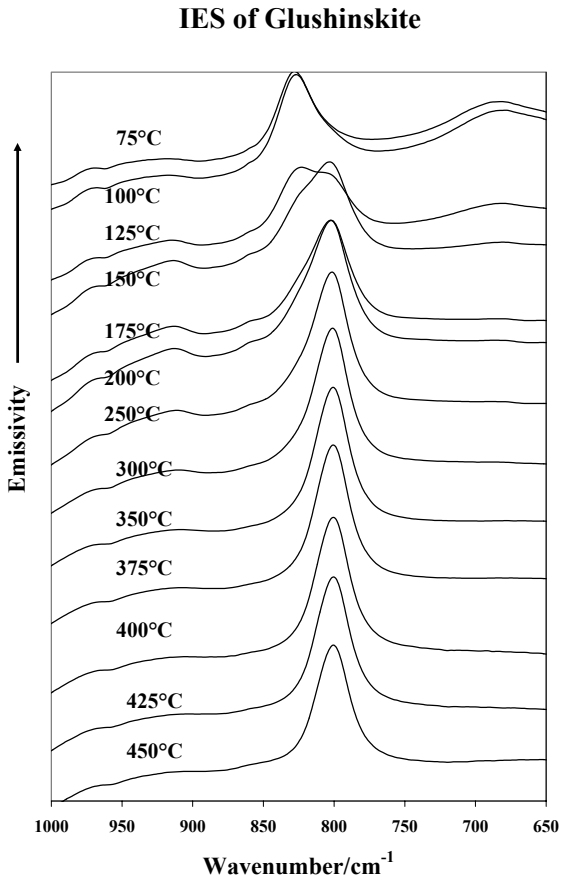
IES of Glushinskite
75°C
100°C
125°C
150°C
175°C
200°C
250°C
300°C
350°C
375°C
400°C
425°C
450°C
Emissivity
1000
950
900
850
800
750
700
650
Wavenumber/cm-1

Figure 7

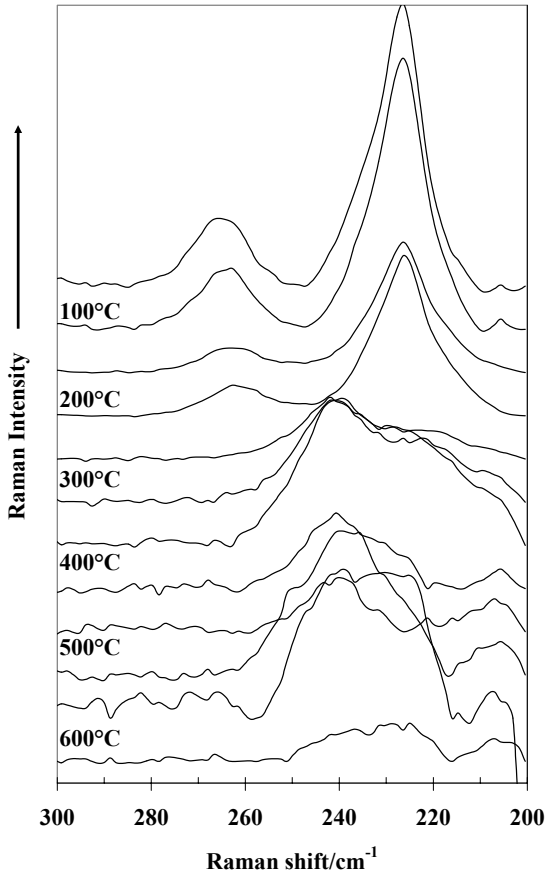
Raman Intensity
100°C
200°C
300°C
400°C
500°C
600°C
300
280
260
240
220
200
Raman shift/cm-1

Figure 9